

# Lymphocyte counting – Error Analysis of Regression versus Bounding Box Detection Approaches

Lin Geng Foo

Engineering Systems and Design (ESD)  
Singapore University of Technology and Design  
lingeng\_foo@mymail.sutd.edu.sg

Alexander Binder

Information Systems Technology and Design (ISTD)  
Singapore University of Technology and Design  
alexander\_binder@sutd.edu.sg

**Abstract**—We consider the problem of counting cell nuclei from celltype-agnostic histopathological stains, exemplified here by the Haematoxylin and Eosin stain. We compare direct estimation by classification and regression against bounding box prediction models for a dataset with relatively low sample sizes. We find from a fine-grained analysis of MSE errors that all models suffer from a substantial underestimation bias. Detection models, while more capricious and sensitive in training, are more robust against underestimation in their optimum. Furthermore the simple idea of combining models from different prediction setups results in large improvements.

## I. INTRODUCTION

Counting cells in histopathological stains is an emerging problem in oncology. Its relevance stems from repeated observations that certain cell types, in particular tumor-infiltrating lymphocytes (TiL) are holding predictive relevance for tumour progression. [1] found correlations between TiLs and disease-free survival in triple negative breast cancers. [2] determined statistically significant correlations between survival and stromal TiL status for estrogen receptor (ER)-negative breast cancer patients. Another line of research [3], [4] investigates correlations between TiLs and therapy responses. Correlations between TiLs and prognostic statistics are also known for other tumor types. For example, [5] found associations between TiLs and overall and progression-free survival in pancreatic cancer.

In this work we focus on the problem of estimating lymphocytes from the standard Haematoxylin and Eosin (H&E) stain, which is commonly used for the assessment of tumors. This task is commonly performed by pathologists according to published guidelines [6].

In the following we remind the reader about a few properties of the counting problem. As common for medical problems, annotations are not easily available unlike in general image problems. Using cloud annotation workers faces acceptance problems with respect to the reliability of the ground truth. Qualified medical experts do not have the time to annotate large databases. This puts limitations on obtaining ground truth in particular for the popular choice of segmentation methods, for which human annotation is substantially more time consuming than providing a mere count.

The Haematoxylin component is known to stain the chromatin in nuclei irrespective of the type of the nucleus, in contrast to cell type specific immunostaining. Thus, lymphocyte counting by algorithms in HE-stained tissues faces the challenge shared with classification problems to discriminate between various types of nuclei.

Notably, the counting problem exhibits a few particular properties among medical imaging tasks.

Firstly, it can be approached by nearly almost all classes of prediction setups encountered in machine learning and deep learning, namely classification, ordinal classification, regression, bounding box detection and segmentation. However, most datasets in the public with segmentation labeling are unsuitable for counting ground truth because they do not discern between different cells of the same type.

Secondly, the distribution of ground truth counts is highly imbalanced. See Figure 1 for the counts from the publicly available CoNSEp dataset. Finally, subsets of interest with high numbers of lymphocytes in a region have low occurrence probability. This makes prediction challenging for the most interesting cases.

Our contributions can be summarized as follows:

- In this paper we compare several deep-learning setups for lymphocyte counting. They are grouped into two categories according to their labeling effort. One is direct prediction by classification and regression. This requires cell counts per patch, and can in practice be achieved by marking cell centers. The second is detection, which requires a bounding box per nucleus.
- We perform a detailed error analysis for all models. We show that all models are generally underestimating the ground truth, which is not expected for those models not predicting via detection.
- We suggest the usage of bin-weighted losses for regression and distance aware cross-entropy losses for classification. We demonstrate that the proposed losses outperform training with MSE and cross-entropy most of the time.
- We propose a hybrid model between regression and classification.

## II. RELATED WORK

Several methods have been proposed to tackle the cell counting problem. They can be roughly grouped into two main categories: direct cell counting methods and cell detection methods. An important difference from a practitioners perspective is their requirement for the labeling of data.

Direct cell counting methods do not output the location of the predicted cells. At best, they can output a density map over the image. One of the first works to focus on the cell counting problem, [7] used linear regression to estimate the density function over the pixels from its dense SIFT features. An integral of the density function over any area can then provide the estimated counts in the area. Subsequently, the density function has been estimated using other different methods, including: Regression forests in [8], Ridge regression with an interactive counting algorithm in [9], Convolutional Neural Networks (CNNs) in [10], redundant counting with CNNs in [11], Self-Attention Module with U-Net in [12], and recently a multi-column extension of the U-Net in [13]. The methods above require dot annotations (representing the center of each cell) during training to generate a ground truth density map. In fact, it was noted in [12] and [11] that providing only the true cell counts was insufficient to yield a correct cell count, as there seems to be too much ambiguity in the loss function.

In [14], only the number of cells in the image is fed to the CNN model during training, which is similar to the regression and classification portions in our work. While training, [14] used the Euclidean loss between the predicted counts and actual counts. They also noted that the cell counting was better done through regression, as the traditional loss functions for classification did not account for the severity of the error, though it was not actually tested. Our work extends [14] through the introduction of new loss functions for regression and classification.

The other way that cell counting has been done is indirectly through cell detection and localization methods, where we can count the output bounding boxes to get cell counts. This also includes segmentation methods. Just to name a few, [15] [16] [17] are all examples of such methods. However, in our work, we decided to test two object detection networks that have been more popular for classifying everyday objects, namely SSD (Or Single-Shot Multibox Detector) [18] and RetinaNet [19].

Our work is also related to ordinal classification methods. [20] introduced a type of distance-aware cross entropy loss for object detection in images using the Gaussian weights. [21] introduced the usage of squared Earth Mover’s distance to training ordered classes. [22] introduced simple methods of reformulating the output layer for ordinal classification, including the use of sigmoid and scaling for regression. To the best of our knowledge, the distance-aware cross entropy loss proposed in this paper has not been considered before for counting problems in histopathology.

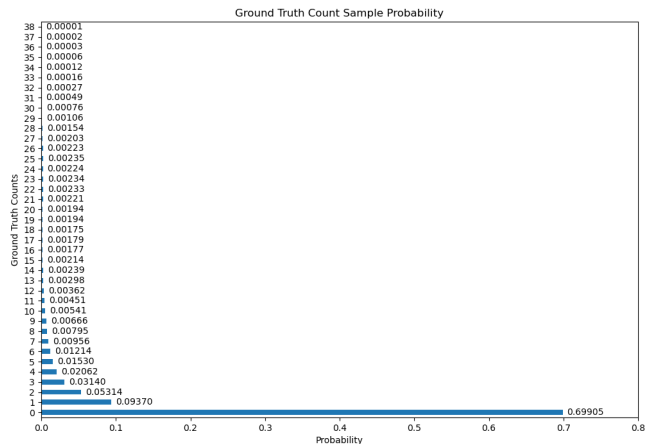


Fig. 1. Sample probabilities over different counts for the CoNSEP dataset.

## III. DATASET AND PREPROCESSING

In fact, we are aware of two datasets which are suitable for histopathological counting. The first is originating from the lysto grand challenge <https://compay19.grand-challenge.org/>. This dataset is using a CD3 and CD8 H+DAB immunostains. While it stains specifically lymphocytes and NK cells, its challenge is to count in the presence of stain diffusion artifacts which frequently can connect neighboring lymphocytes. The second dataset, CoNSEP, stems from the work [23] and is based on the H&E stain which we intend to experiment on.

The dataset consists of 41 images of size  $1000 \times 1000$  such that each pixel being labelled as belonging to the background tissue, or belonging to a type of nuclei. Additionally, the pixels are grouped into separate nuclei, which therefore provides a labelling suitable for counting ground truth and for bounding box detection. The types of nuclei are as follows: normal epithelial, malignant/dysplastic epithelial, fibroblast, muscle, inflammatory, endothelial or miscellaneous.

As we focus on the lymphocyte counting problem, we only keep the inflammatory nuclei, and designate everything else as background. There were a total of 5579 lymphocytes in the entire dataset.

We split each image into smaller patches for training, using a sliding window of size  $120 \times 120$  and a stride of 8. We counted a cell to be within the patch if the cell centers (defined as the mean of all pixel coordinates of the cell) were at least 5 pixels inward from the border. This gave us 12321 patches per image. Overall, the number of cells in each patch ranged from 0 – 38. The histogram of sample frequencies can be seen in Figure 1. It can be clearly seen that many of the patches have low counts. The overall mean count per patch is 1.64. This is an important detail that would motivate our choice of loss function later on.

The 41 images were split into training (27 images) and test (14 images) sets. This corresponds to having 3941 inflammatory nuclei in the training set and 1638 in the test set. During

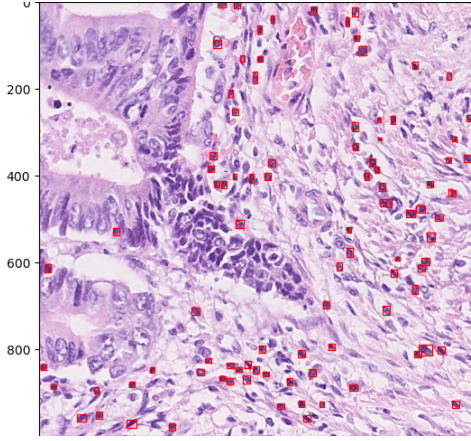


Fig. 2. Sample of a  $1000 \times 1000$  image from the CoNSEP dataset with bounding boxes in red

training, we also added rotations and horizontal/vertical flips to the data.

#### A. Binning the counts

The classifiers require the counts to be binned. Furthermore for the subsequent error analysis, we like to observe the errors for intervals of different mean sizes. Therefore we further processed the data to group the counts into appropriate bins, with at least 1000 samples in each bin whenever possible. The procedure can roughly be described as such: We first get the histogram showing the number of patches that exist for each ground truth count, and then group "counts" together into bins, starting from the higher counts, such that each bin has at least 1000 patches. Through this process, we managed to map all counts of 0-38 into 23 bins.

#### B. Bounding boxes

For the purpose of training our bounding box detectors, we also labelled the bounding box of each cell in  $[y_{min}, x_{min}, y_{max}, x_{max}]$  format, where each coordinate is the max/min value of the cell's coordinates in a dimension. When generating the  $120 \times 120$ -sized patches, if the cell's center is in the patch but parts of it are not, we crop the bounding box to fully fit inside the patch.

We show a sample of a full  $1000 \times 1000$  image in Fig 2, with the lymphocytes in red bounding boxes.

### IV. MODELS

We experimented with three different types of models, namely regression, classification and object detection models.

#### A. Regression Models

We conduct our experiments on the following 6 architectures: GoogleNet [24], ResNet-18 [25], ResNet-101 [25], DenseNet-121 [26], Inception-v3 [27] and VGG-11 [28]. Pretrained models from the Pytorch model zoo were used. We then experimented with three different configurations for the final layer. 1) A fully connected layer to a single value, followed by a ReLU to make the output non-negative. 2)

A fully connected layer to a single value, followed by a sigmoid, then a scaling of 100. 3) A fully connected layer to a single value, followed by a sigmoid, then a scaling of 38. We term these three configurations as ReLU, Sig-100 and Sig-38 respectively.

Instead of using a single model, we train 4 copies of each model for 30 epochs, with each copy leaving out a different part of the training set for validation purposes. At test time, we load the best-performing weights for each copy, run the test images through all 4 of them and average the outputs to give a final count prediction.

1) *Loss*: For these regression models, the training loss is the root mean bin-wise mean-squared error (RMBMSE). Roughly speaking, we just gather MSE of the ground truths in each bin, and then average them. Now we define it formally. Let there be a batch of  $n$  outputs from the model,  $x_1, x_2, \dots, x_n$ , which are estimates of the counts, with ground truths  $y_1, y_2, \dots, y_n \in [0, m - 1]$ . Let  $h$  be the function that maps a count  $i$  to its corresponding bin  $B_i$ . The loss (where  $L_{bin}$  stands for the RMBMSE loss) is:

$$L_{bin} = \left[ \frac{1}{m} \sum_{j=1}^m \sum_{i=1}^n (x_i - y_i)^2 \frac{\mathbf{1}\{h(y_i) = j\}}{|B_j|} \right]^{0.5} \quad (1)$$

$$|B_j| = \sum_i \mathbf{1}\{h(y_i) = j\} \quad (2)$$

Where  $B_j$  is the bin with the ground truth label  $j$ . This loss is designed to steer the model to focus slightly more on the "rarer" images (which are the images with higher counts). The division by bin counts helps to reduce the weight on common samples and increases the weight on rarer samples, such that more emphasis is placed on getting the higher counts right, as compared to the usual MSE loss. If the counts of cells in the patches were uniformly spread among 0-38, this loss would be similar to MSE.

#### B. Classification Models

We reuse the same 6 architectures and pretrained models as the regression models. We also adopt the same procedure and train 4 copies of each model before aggregating their outputs at test time. For the final layer, we had two configurations: 1) a fully connected layer to 39 logits (one class per count) followed by softmax 2) a fully connected layer to 23 logits (one class per bin) before applying softmax. We name these configurations as CE-count and CE-bin respectively. For CE-bin, there is a small additional step before applying the loss as we need to retrieve the counts from the class predictions. To do this, we assign each class prediction to be the mean of counts associated with each bin.

1) *Loss*: For these classification models, the training loss is the distance-weighted cross entropy. For the sake of simplicity, let there be just one output  $x$  where  $x$  is a vector of size  $m$ , with ground truth count  $y$ . Let  $f$  be the function mapping a

TABLE I  
MSE FOR REGRESSION MODELS.  $L_{bin}$  AND MSE IN THE SECOND ROW DENOTE THE LOSSES USED FOR TRAINING.

Architecture	ReLU		Sig-100		Sig-38	
	$L_{bin}$	MSE	$L_{bin}$	MSE	$L_{bin}$	MSE
GoogleNet	<b>2.68</b>	2.75	<b>3.04</b>	3.15	<b>2.46</b>	3.25
ResNet-18	2.84	<b>2.81</b>	<b>2.79</b>	2.95	<b>2.89</b>	3.09
ResNet-101	<b>3.09</b>	3.10	<b>3.07</b>	3.18	<b>2.98</b>	3.27
DenseNet-121	<b>2.84</b>	2.95	<b>2.84</b>	2.89	3.17	<b>3.07</b>
Inception-v3	2.98	<b>2.81</b>	<b>2.65</b>	2.69	<b>2.73</b>	2.97

TABLE II  
MSE FOR CLASSIFICATION MODELS.  $L_{DWCE}$ , CE-BIN AND CE-COUNT DENOTE THE LOSSES USED.

Architecture	$L_{DWCE}$	CE-bin	CE-count
GoogleNet	<b>3.05</b>	3.56	3.65
ResNet-18	<b>3.01</b>	3.48	3.33
ResNet-101	3.30	<b>2.87</b>	3.51
DenseNet-121	<b>3.00</b>	3.10	3.13
Inception-v3	3.23	<b>2.98</b>	3.08

bin to the mean value of counts it represents (for a bin  $i$  with counts 26 and 27,  $f(i) = 26.5$ ).

$$L_{DWCE} = \sum_{i \neq y} (f(i) - y)^2 [-\log(1 - p_i)] \quad (3)$$

The idea behind this loss function is to penalize the prediction based on its distance to the ground truth, as well as its confidence in its prediction. As the distance to the ground truth  $(f(i) - y)^2$  increases, our loss increases. Given an incorrect prediction  $i \neq y$ , the loss should also increase if  $p_i$  (and therefore  $-\log(1 - p_i)$ ) increases, as we are overly confident in the wrong bin. We also note that a perfect prediction  $p_y = 1, p_{i \neq y} = 0$  gives us a loss of 0.

### C. Object detection Models

We were also curious to know how well object detectors fared. We trained two object detectors, namely RetinaNet and SSD. For both of them, we ran the training for 500 epochs, and took the model that did the best on a held-out validation set, based on the RBMSE metric. After getting the best model, we then ran experiments on the validation set, to tune for the best score threshold parameter for each of the RBMSE and mAP metrics. We experimented for a value in  $[0, 0.5]$  in intervals of 0.05. To make things simple, we fixed a maximum of 200 detections per image for both models.

1) *RetinaNet*: We trained on a RetinaNet model that was pre-trained on COCO. We left the box sub-network untouched and changed only the number of classes in the box sub-network. We also used their proposed Focal Loss during training, setting  $\gamma = 2, \alpha = 0.25$ .

We used an Adam Optimizer with a learning rate of  $10e-3$ , with a scheduler that decreased by a factor of 0.1 after 3 epochs of plateauing. Importantly, we re-scaled the patches to be of size  $608 \times 608$  to fit the size of the network. We

TABLE III  
RBMSE FOR REGRESSION MODELS.  $L_{bin}$  AND MSE IN THE SECOND ROW DENOTE THE LOSSES USED FOR TRAINING.

Architecture	ReLU		Sig-100		Sig-38	
	$L_{bin}$	MSE	$L_{bin}$	MSE	$L_{bin}$	MSE
GoogleNet	<b>5.21</b>	5.85	<b>5.28</b>	6.79	<b>3.56</b>	6.90
ResNet-18	5.51	<b>5.44</b>	<b>4.86</b>	5.00	<b>5.96</b>	6.43
ResNet-101	<b>6.17</b>	6.64	<b>5.84</b>	7.16	<b>6.00</b>	7.55
DenseNet-121	<b>4.76</b>	7.30	<b>5.23</b>	5.71	6.91	<b>6.81</b>
Inception-v3	<b>5.88</b>	6.03	<b>5.21</b>	5.32	<b>5.04</b>	5.15

TABLE IV  
RBMSE FOR CLASSIFICATION MODELS.  $L_{DWCE}$ , CE-BIN AND CE-COUNT DENOTE THE LOSSES USED.

Architecture	$L_{DWCE}$	CE-bin	CE-count
GoogleNet	<b>5.51</b>	7.17	7.37
ResNet-18	7.38	<b>6.20</b>	7.06
ResNet-101	7.41	<b>5.52</b>	8.00
DenseNet-121	<b>5.95</b>	5.97	6.82
Inception-v3	7.15	<b>5.52</b>	6.21

TABLE V  
METRICS FOR DETECTION MODELS. MSE AND RBMSE IS THE SAME MEASURE AS REPORTED FOR THE OTHER MODEL TYPES.

Architecture	MSE	RBMSE	mAP	Precision	Recall
RetinaNet-0.05	25.9k	232	0.618	0.039	0.876
RetinaNet-0.20	8.74	<b>4.33</b>	0.534	0.653	0.638
SSD	9.71	6.88	0.616	0.705	0.686

also used non-maximum suppression with a threshold of 0.5. After obtaining our final RetinaNet model, we found that a score threshold of 0.2 minimized the RBMSE metric, and a score threshold of 0.05 minimized the mAP metric. In Table V below, the RetinaNet-0.20 and RetinaNet-0.05 refer to the same model under these different score thresholds.

2) *SSD*: We trained on a SSD-300 model that was pre-trained on VOC 2007 and 2012. We used SGD with a learning rate of  $1e-3$ , momentum of 0.9 and weight decay of  $5e-4$ . We also re-scaled patches to be of size  $300 \times 300$  to fit the requirements of the pre-trained network. Non-maximum suppression with a threshold of 0.45 was used. For our final SSD model, we found that a score threshold of 0.2 and setting a maximum of 200 detections minimized both the RBMSE and mAP metrics.

## V. EXPERIMENTAL RESULTS

### A. Metrics

Our final evaluation metric used is the root mean binwise MSE (RBMSE), introduced previously in Eqn 1. We designed it such that a model can have a lower error if it manages to perform well on prediction on the higher counts, as well as on the lower counts. We also provide the usual MSE metric for comparison.

## B. Results for regression

We refer the reader to Table I and Table III for our results on the regression models. Our loss  $L_{RMBMSE}$  was able to reduce both the MSE and RMBMSE test losses for the regression models. This is especially so for the Sig-100 configuration, where all models showed some improvement over the MSE-trained counterpart.

In fact, we observe that when we train using the RMBMSE loss, we are also minimizing the test MSE metric well. However, when we train using the MSE loss, the test RMBMSE loss is sometimes not well controlled and there is sometimes a large difference in this metric, eg. GoogleNet-Sig-38 and DenseNet121-ReLU in Table III.

Something else interesting we found was that when using MSE as the training loss, the Sig-38 configuration was generally outperformed by both the Sig-100 and the ReLU model. This is interesting as we would have expected the Sig-38 to do just as well, if not better (which was the inherent assumption in [22]). Looking at the error plots, we observe that the Sig-38 configuration tends to consistently underestimate the counts more than the Sig-100 configuration.

Lastly, a conscientious reader might have also realized that we have left out the VGG-11 in our table of results, as the VGG-11 architecture was not able to learn the task successfully and predicted "0" most of the time (especially so for regression), leading to the statistics just capturing the variance in the test data.

## C. Results for classification

Overall, our classifiers performed slightly worse than the regression models in both MSE and RMBMSE, which is to be expected.

From our results in Table II and Table IV, we found that binning the counts before classification was generally helpful in lowering both the MSE and RMBMSE. This is in spite of having to approximate predictions through bin averages, showing that our approach in binning before classification was a helpful one. In particular, the decrease in RMSE from CE-count to CE-bin is also a substantial one. This shows that a using classes with less samples per class results in higher losses. This can be observed in Fig 3, and it appears even more substantially in the DenseNet models in Fig 6.

## D. Results for detection models

Referring to Table V, we found that when the threshold scores were optimized for the RMBMSE metric, the RetinaNet-0.20 model performed better on the counting task, having a slightly smaller MSE and a much significantly smaller RMBMSE. Interestingly, this is in spite of RetinaNet-0.20 having a lower mAP, precision and recall. We believe that this might be attributed to the RetinaNet-0.20 striking a better balance between over-estimation and under-estimation at each bin. This pattern can be observed in the error plots in Fig 5.

Considering that these cell detectors are more strongly supervised as they also get the ground truth bounding boxes

during training, this is a relatively poor performance by the cell detectors.

We also found that the two models were fundamentally quite different in their precision-recall trade-off. The the SSD model had a rather balanced precision (0.705) and recall score (0.686), and the mAP was maximized at roughly the same score threshold as the RMBMSE metric. On the other hand, the RetinaNet model had to choose between optimizing for mAP or for RMBMSE. Setting the score threshold to 0.05 led to a high recall (0.876) but very low precision (0.039), while setting it to 0.20 balanced the recall with the precision. We emphasize that this is the result of the inherent differences in the model architectures, as there were more anchor boxes in the RetinaNet's architecture (about 100k), compared to 8732 in the SSD.

Intuitively, the estimation would be the best when precision and recall are about similar, such that on average, the expected number of false positives and false negatives are around the same. The data above affirms this.

## E. Analysis of the Error Plots

We refer here to Figures 3, 4, 6, and 5. We can see that the errors are consistently due to underestimation, even when MSE loss does not enforce such a bias. We observe that regression models do not fare better for ground truths with high lymphocyte counts compared to classification models trained with binning (CE-bin) or weighted loss  $L_{DWCE}$ . However the regression models tend to be better in the lower ranges of ground truths.

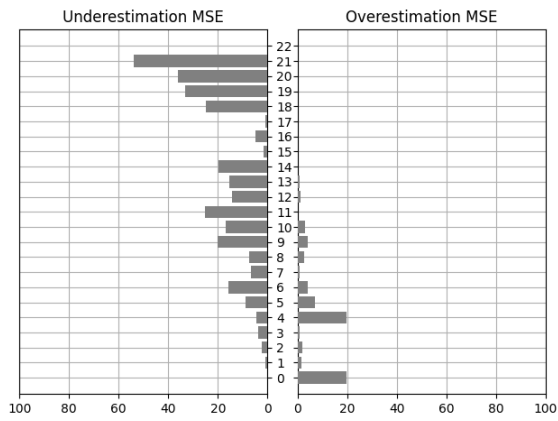
Regarding detection models in Figure 5 we see firstly, that a large number of region proposals in RetinaNet helps substantially.

Comparing direct against detection models we notice that the strength of a properly trained detection model is its relatively lower underestimation bias for large counts. Furthermore, detection models tend to hallucinate more lymphocytes, as can be seen by comparing the overestimation MSE.

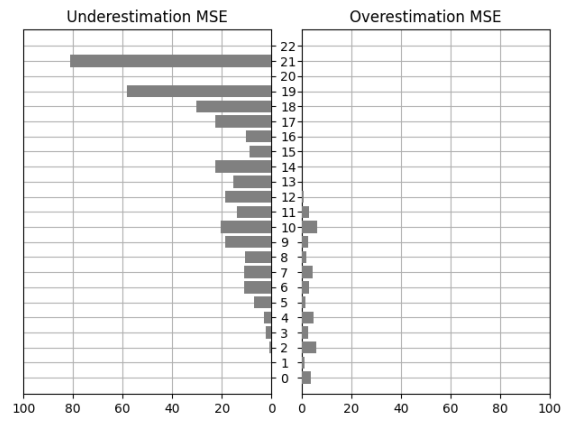
## F. Results for hybrid models

We combined a regression, a classification model and a detection model together in a pairwise manner. The former two were chosen from DenseNet models. We picked the Sig-100  $L_{RMBMSE}$ -trained version for the regression model, and the CE-bin version for our classification model (we picked one out of the 4 trained copies used for testing). For the detection model, we used the Retina-0.20 configuration that performed the best. We tried two simple methods: taking the mean of predictions, and taking the maximum. The results are shown in Table VI.

The results are very promising. Starting from a RMBMSE of 5.23 and 5.97 for the single classification/regression models, which are not the best available ones, just using Plain averaging gave results that were among the lowest among all our models with a RMBMSE of 3.72. Taking the maximum improved the MSE and RMBMSE scores even further, yielding the best test scores so far, with a MSE of 2.33 and a RMBMSE

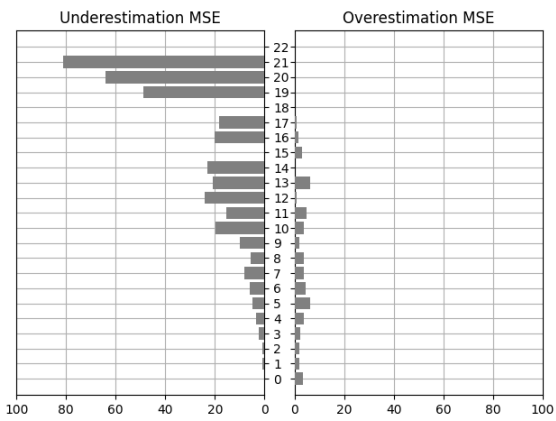


(a) The error plot of GoogleNet model trained using CE-bin

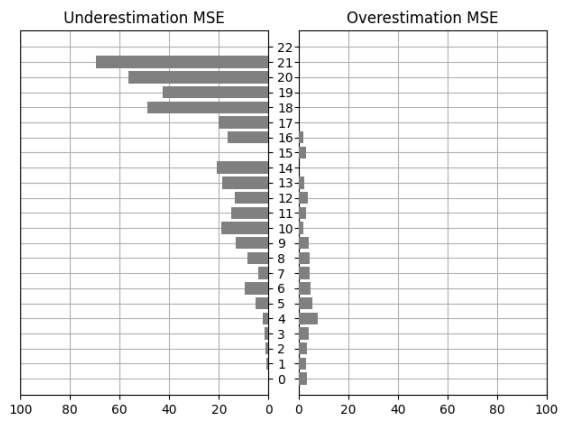


(b) The error plot of GoogleNet model trained using  $L_{DWCE}$

Fig. 3. Error analysis for classification models.

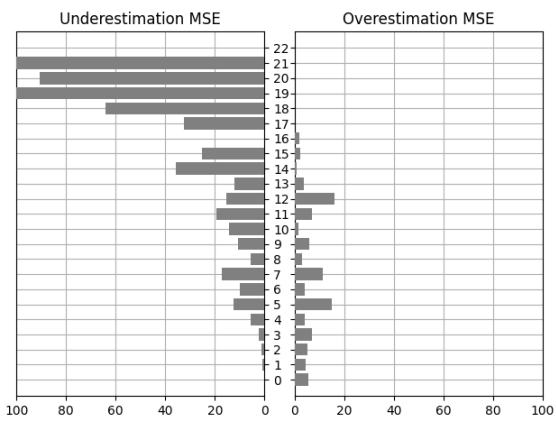


(a) GoogleNet model with a final ReLU layer trained using  $MSE$

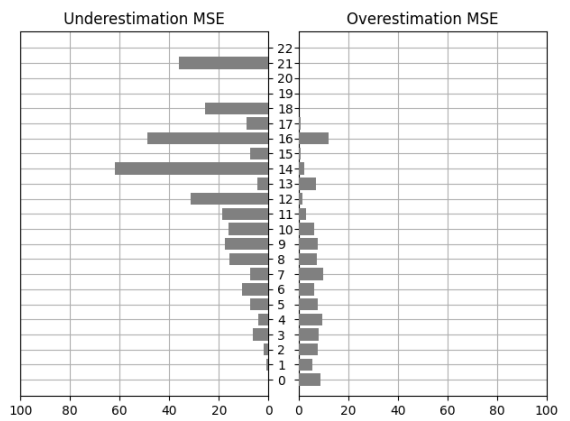


(b) GoogleNet model with a final ReLU layer trained using  $L_{bin}$

Fig. 4. Error analysis for regression models.



(a) The error plot of SSD



(b) The error plot of RetinaNet-0.2

Fig. 5. Error analysis for detection models

of 3.32. The other combinations of "Det,Reg" and "Det, Cls" also found similar improvements.

While uncommon otherwise, taking the max is beneficial here because all our models tend to underestimate (the error

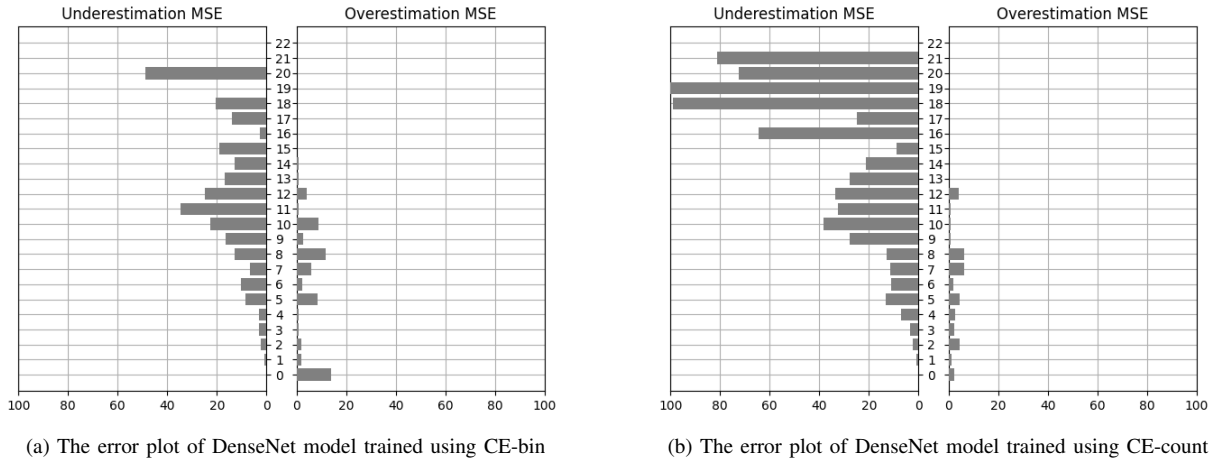


Fig. 6. Error analysis for classification models II, for a different base neural net, comparing CE-bin versus CE-count, which is the naive classification over all counts.

TABLE VI  
METRICS FOR HYBRID MODELS WITH A MIX OF CLASSIFICATION (CLS), REGRESSION (REG) AND DETECTION (DET). MSE AND RMBMSE IS THE SAME MEASURE AS REPORTED FOR THE OTHER MODEL TYPES.

Mix	Method	MSE	RMBMSE
Cls, Reg	Average	2.42	3.72
Cls, Reg	Max	2.33	3.32
Det, Reg	Average	4.25	8.73
Det, Reg	Max	2.49	3.93
Det, Cls	Average	4.36	8.63
Det, Cls	Max	2.51	4.31

plots are heavily slanting to the left). Taking the max between two models helps to mitigate this bias.

## VI. CONCLUSION

In this work, we compared different approaches to counting lymphocytes on a HE stain. Future work would include testing our newly proposed losses on larger datasets that are differently distributed compared to the CoNSeP dataset. We also suggest using hybrid models as a promising avenue for improving performance.

## REFERENCES

- [1] C. Denkert, G. von Minckwitz, S. Darb-Esfahani, B. Lederer, B. I. Heppner, K. E. Weber, J. Budczies, J. Huober, F. Klauschen, J. Furlanetto, W. D. Schmitt, J.-U. Blohmer, T. Karn, B. M. Pfitzner, S. Kümmel, K. Engels, A. Schneeweiss, A. Hartmann, A. Noske, P. A. Fasching, C. Jackisch, M. van Mackelenbergh, P. Sinn, C. Schem, C. Hanusch, M. Untch, and S. Loibl, "Tumour-infiltrating lymphocytes and prognosis in different subtypes of breast cancer: a pooled analysis of 3771 patients treated with neoadjuvant therapy," *The Lancet Oncology*, vol. 19, no. 1, pp. 40–50, Jan 2018. [Online]. Available: [https://doi.org/10.1016/S1470-2045\(17\)30904-X](https://doi.org/10.1016/S1470-2045(17)30904-X)
- [2] S. Kurozumi, H. Matsumoto, M. Kurozumi, K. Inoue, T. Fujii, J. Horiguchi, K. Shirabe, T. Oyama, and H. Kuwano, "Prognostic significance of tumour-infiltrating lymphocytes for oestrogen receptor-negative breast cancer without lymph node metastasis," *Oncology letters*, vol. 17, no. 3, pp. 2647–2656, Mar 2019, 30867728[pmid]. [Online]. Available: <https://pubmed.ncbi.nlm.nih.gov/30867728>
- [3] T. Watanabe, A. I. Hida, N. Inoue, M. Imamura, Y. Fujimoto, K. Akazawa, S. Hirota, and Y. Miyoshi, "Abundant tumor infiltrating lymphocytes after primary systemic chemotherapy predicts poor prognosis in estrogen receptor-positive/her2-negative breast cancers," *Breast Cancer Research and Treatment*, vol. 168, no. 1, pp. 135–145, Feb 2018. [Online]. Available: <https://doi.org/10.1007/s10549-017-4575-z>
- [4] T. Khoury, V. Nagrale, M. Opyrchal, X. Peng, D. Wang, and S. Yao, "Prognostic significance of stromal versus intratumoral infiltrating lymphocytes in different subtypes of breast cancer treated with cytotoxic neoadjuvant chemotherapy," *Applied immunohistochemistry & molecular morphology : AIMM*, vol. 26, no. 8, pp. 523–532, Sep 2018, 28187033[pmid]. [Online]. Available: <https://pubmed.ncbi.nlm.nih.gov/28187033>
- [5] R. C. Miksch, M. B. Schoenberg, M. Weniger, F. Bösch, S. Ormanns, B. Mayer, J. Werner, A. V. Bazhin, and J. G. D'Haese, "Prognostic impact of tumor-infiltrating lymphocytes and neutrophils on survival of patients with upfront resection of pancreatic cancer," *Cancers*, vol. 11, no. 1, p. 39, Jan 2019, 30609853[pmid]. [Online]. Available: <https://pubmed.ncbi.nlm.nih.gov/30609853>
- [6] M. V. Dieci, N. Radosevic-Robin, S. Fineberg, G. van den Eynden, N. Ternes, F. Penault-Llorca, G. Pruneri, T. M. DAlfonso, S. Demaria, C. Castaneda, J. Sanchez, S. Badve, S. Michiels, V. Bossuyt, F. Rojo, B. Singh, T. Nielsen, G. Viale, S.-R. Kim, S. Hewitt, S. Wienert, S. Loibl, D. Rimm, F. Symmans, C. Denkert, S. Adams, S. Loi, and R. Salgado, "Update on tumor-infiltrating lymphocytes (tils) in breast cancer, including recommendations to assess tilis in residual disease after neoadjuvant therapy and in carcinoma in situ: A report of the international immuno-oncology biomarker working group on breast cancer," *Seminars in Cancer Biology*, vol. 52, pp. 16 – 25, 2018, immuno-oncological biomarkers. [Online]. Available: <http://www.sciencedirect.com/science/article/pii/S1044579X17302171>
- [7] V. Lempitsky and A. Zisserman, "Learning to count objects in images," in *Proceedings of the 23rd International Conference on Neural Information Processing Systems - Volume 1*, ser. NIPS10. Red Hook, NY, USA: Curran Associates Inc., 2010, p. 13241332.
- [8] L. Fiaschi, U. Koethe, R. Nair, and F. A. Hamprecht, "Learning to count with regression forest and structured labels," in *Proceedings of the 21st International Conference on Pattern Recognition (ICPR2012)*, 2012, pp. 2685–2688.
- [9] C. Arteta, V. Lempitsky, J. A. Noble, and A. Zisserman, "Interactive object counting," in *European Conference on Computer Vision*, 2014.
- [10] W. Xie, J. A. Noble, and A. Zisserman, "Microscopy cell counting and detection with fully convolutional regression networks," *Computer Methods in Biomechanics and Biomedical Engineering: Imaging & Visualization*, vol. 6, no. 3, pp. 283–292, 2018. [Online]. Available: <https://doi.org/10.1080/21681163.2016.1149104>
- [11] J. P. Cohen, H. Z. Lo, and Y. Bengio, "Count-ception: Counting by

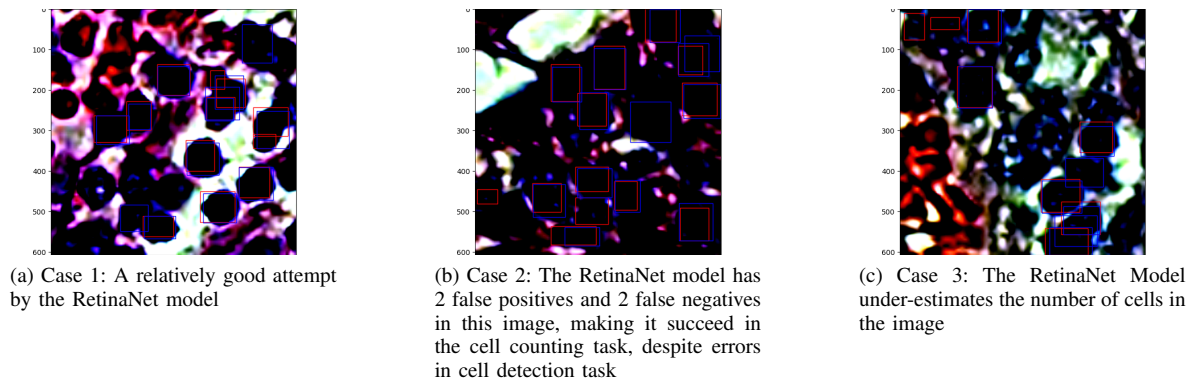


Fig. 7. Predictions from our trained RetinaNet-0.20 model are in blue, while the ground truth bounding boxes are in red.

- fully convolutional redundant counting,” *CoRR*, vol. abs/1703.08710, 2017. [Online]. Available: <http://arxiv.org/abs/1703.08710>
- [12] Y. Guo, J. Stein, G. Wu, and A. Krishnamurthy, “Sau-net: A universal deep network for cell counting,” in *Proceedings of the 10th ACM International Conference on Bioinformatics, Computational Biology and Health Informatics*, ser. BCB 19. New York, NY, USA: Association for Computing Machinery, 2019, p. 299306. [Online]. Available: <https://doi.org/10.1145/3307339.3342153>
- [13] N. Jiang and F. Yu, “Multi-column network for cell counting,” *OSA Continuum*, vol. 3, no. 7, pp. 1834–1846, Jul 2020. [Online]. Available: <http://www.osapublishing.org/osac/abstract.cfm?URI=osac-3-7-1834>
- [14] Y. Xue, N. Ray, J. Hugh, and G. Bigras, “Cell counting by regression using convolutional neural network,” in *Computer Vision – ECCV 2016 Workshops*, G. Hua and H. Jégou, Eds. Cham: Springer International Publishing, 2016, pp. 274–290.
- [15] C. Arteta, V. Lempitsky, J. A. Noble, and A. Zisserman, “Learning to detect cells using non-overlapping extremal regions,” in *Medical Image Computing and Computer-Assisted Intervention – MICCAI 2012*, N. Ayache, H. Delingette, P. Golland, and K. Mori, Eds. Berlin, Heidelberg: Springer Berlin Heidelberg, 2012, pp. 348–356.
- [16] S. U. Akram, J. Kannala, L. Eklund, and J. Heikkilä, “Cell segmentation proposal network for microscopy image analysis,” in *Deep Learning and Data Labeling for Medical Applications*, G. Carneiro, D. Mateus, L. Peter, A. Bradley, J. M. R. S. Tavares, V. Belagiannis, J. P. Papa, J. C. Nascimento, M. Loog, Z. Lu, J. S. Cardoso, and J. Cornebise, Eds. Cham: Springer International Publishing, 2016, pp. 21–29.
- [17] O. Ronneberger, P. Fischer, and T. Brox, “U-net: Convolutional networks for biomedical image segmentation,” in *Medical Image Computing and Computer-Assisted Intervention – MICCAI 2015*, N. Navab, J. Hornegger, W. M. Wells, and A. F. Frangi, Eds. Cham: Springer International Publishing, 2015, pp. 234–241.
- [18] W. Liu, D. Anguelov, D. Erhan, C. Szegedy, S. E. Reed, C. Fu, and A. C. Berg, “SSD: single shot multibox detector,” *CoRR*, vol. abs/1512.02325, 2015. [Online]. Available: <http://arxiv.org/abs/1512.02325>
- [19] T. Lin, P. Goyal, R. B. Girshick, K. He, and P. Dollár, “Focal loss for dense object detection,” *CoRR*, vol. abs/1708.02002, 2017. [Online]. Available: <http://arxiv.org/abs/1708.02002>
- [20] H. Law and J. Deng, “Cornersnet: Detecting objects as paired keypoints,” *CoRR*, vol. abs/1808.01244, 2018. [Online]. Available: <http://arxiv.org/abs/1808.01244>
- [21] L. Hou, C. Yu, and D. Samaras, “Squared earth mover’s distance-based loss for training deep neural networks,” *CoRR*, vol. abs/1611.05916, 2016. [Online]. Available: <http://arxiv.org/abs/1611.05916>
- [22] C. Beckham and C. Pal, “A simple squared-error reformulation for ordinal classification,” 2016.
- [23] P. Naylor, M. La, F. Reyat, and T. Walter, “Nuclei segmentation in histopathology images using deep neural networks,” in *2017 IEEE 14th International Symposium on Biomedical Imaging (ISBI 2017)*, 2017, pp. 933–936.
- [24] C. Szegedy, W. Liu, Y. Jia, P. Sermanet, S. Reed, D. Anguelov, D. Erhan, V. Vanhoucke, and A. Rabinovich, “Going deeper with convolutions,” in *Computer Vision and Pattern Recognition (CVPR)*, 2015. [Online]. Available: <http://arxiv.org/abs/1409.4842>
- [25] K. He, X. Zhang, S. Ren, and J. Sun, “Deep residual learning for image recognition,” *CoRR*, vol. abs/1512.03385, 2015. [Online]. Available: <http://arxiv.org/abs/1512.03385>
- [26] G. Huang, Z. Liu, and K. Q. Weinberger, “Densely connected convolutional networks,” *CoRR*, vol. abs/1608.06993, 2016. [Online]. Available: <http://arxiv.org/abs/1608.06993>
- [27] C. Szegedy, V. Vanhoucke, S. Ioffe, J. Shlens, and Z. Wojna, “Rethinking the inception architecture for computer vision,” *CoRR*, vol. abs/1512.00567, 2015. [Online]. Available: <http://arxiv.org/abs/1512.00567>
- [28] K. Simonyan and A. Zisserman, “Very deep convolutional networks for large-scale image recognition,” *arXiv 1409.1556*, 09 2014.